Available online at www.sciencedirect.com
ScienceDirect
Journal of the European Ceramic Society 29 (2009) 1083–1092
www.elsevier.com/locate/jeurceramsoc

Sandwich materials formed by thick alumina tapes and thin-layered alumina–aluminium titanate structures shaped by EPD

Begoña Ferrari, Alberto Bartret, Carmen Baudín *

Instituto de Cerámica y Vidrio, CSIC, Kelsen 5, 28049 Madrid, Spain

Received 1 June 2008; received in revised form 11 July 2008; accepted 18 July 2008
Available online 4 September 2008

Abstract

The objective of this work was to analyse the potential of the alumina (Al_2O_3)–titania (TiO_2) system to fabricate laminates with very thin deflecting layers. Alumina–aluminium titanate structures formed by thick self-supported alumina tapes (400 μm) joined together by layered alumina–aluminium titanate structures shaped by EPD have been developed and their mechanical response has been evaluated as a function of the thickness of the layered structures. For this purpose the stability of alumina and alumina–titania suspensions in ethanol was optimized and the EPD parameters to control the growth of layers on non-conductive substrates were analysed. Two different sandwich structures formed by external alumina tapes joined by multilayer systems built by EPD were fabricated. Differences between the multilayer systems were based on the thickness of the layers. Large portions of the central parts of the laminates with thicker layers remained un-fractured while multiple delaminations were observed in the central parts of the specimens with thinner layers that presented wood-like fracture. The fracture modes were reflected in the load-displacement curves as higher loads were needed to fracture the more resistant thicker ligaments whereas larger displacements were admitted by the specimens with thinner layers due to multiple delaminations.

Keywords: A. Shaping; B. Composites; C. Toughness and toughening; D. Al_2O_3; Al_2TiO_5; E. Structural applications

1. Introduction

One of the most promising new approaches to avoid the lack of mechanical reliability of ceramics is that of layered materials. Since the seminal work by Clegg et al.[1] ceramic–ceramic layered composites have been designed and processed on the basis of weak interfaces between layers to originate crack deflection (e.g., see references[2–5]). Such materials present high values of work of fracture and apparent toughness under loads perpendicular to the layers.

In previous works[6–9] alumina–aluminium titanate based ceramic–ceramic laminates designed to reach high work of fracture and apparent toughness were studied. They alternated relatively thick (≈500–2100 μm) stiff and brittle external and internal layers with thin (≈150–300 μm) compliant internal ones. In particular, when highly microcracked[8,9] internal layers were present, multiple crack deflection at the microstructural scale occurred, thus, delamination lengths were limited and structural integrity was not lost due to delamination. It was demonstrated that the stiff and brittle external layers carried load whereas the microcracked ones supported damage. Large strains to fracture with high work of fracture (≈60–125 J m^{-2}) and apparent toughness (10–22 MPa m$^{1/2}$) values, depending on the laminate design, were obtained.

In order to extend this laminate concept to coatings, structures containing much thinner layers have to be envisaged. Moreover, the reduction of the thickness of the compliant composite layers would lead to the increase of the relative volume fraction of the load carrying alumina layers, as occurs in natural structures such as shells.

The objective of this work was to analyse the potential of the alumina (Al_2O_3)–titania (TiO_2) system to fabricate laminates with very thin deflecting layers. The proposed processing route was the piling up of pure alumina cast tapes separated by structures formed by alternate very thin layers of Al_2O_3 (A) and Al_2O_3/TiO_2 (AT) in order to attain external mechanical

* Corresponding author. Tel.: +34 917355840; fax: +34 917355843.
E-mail address: cbaudin@icv.csic.es (C. Baudín).

0955-2219/$ – see front matter © 2008 Elsevier Ltd. All rights reserved.
doi:10.1016/j.jeurceramsoc.2008.07.048

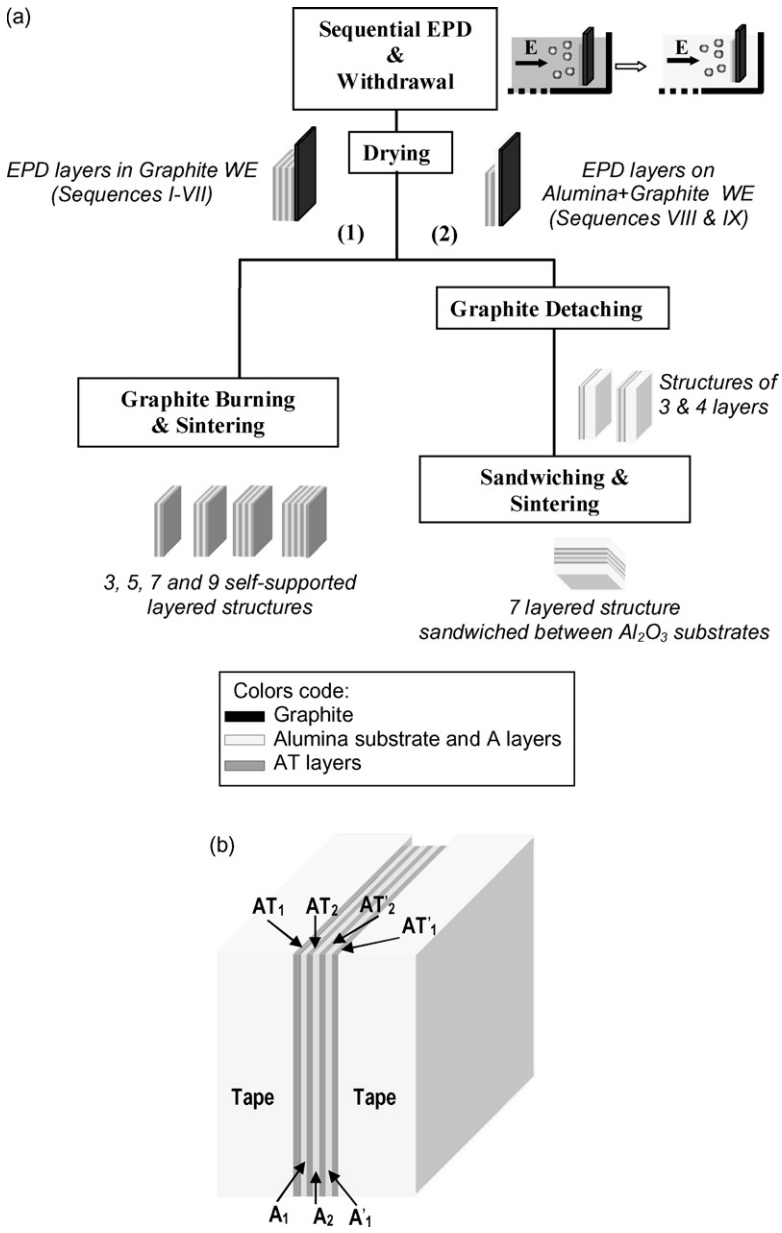

Fig. 1. Designed and fabricated structures and processing parameters. (a) Flow chart for the fabrication of self-supported layered films (1) and sandwich structures (2). (b) Schematics of the green sandwich structures.

resistance together with internal deflection of the cracks. The processing technique selected to get the thin-layered structure was electrophoretic deposition (EPD). An alumina–titania composition richer in titania than that of aluminium titanate was chosen in order to enhance the high temperature diffusion of titania into alumina and, consequently, to facilitate the joining. In this preliminary work, sandwich structures formed by two external alumina tapes were studied.

EPD is the most accurate technique to shape structures alternating thin layers with different compositions.[10] Electrically conducting substrates have been considered a pre-requisite for the electrophoretic deposition until recently. However, Besra et al.[11] have demonstrated the feasibility of deposition on non-conducting porous substrates; a "conductive path" between the electrode and the particles in suspension is established once the porous substrate is saturated by the solvent. In such cases, deposition depends on the substrate porosity. A threshold porosity value can be determined for each substrate above which deposition by EPD is possible.

In order to establish the optimum conditions to reach sequences of alternated A and AT layers, the kinetics of EPD of slips constituted by pure alumina and by alumina–titania mixtures on graphite and on alumina substrates was first studied and self-supported monolithic and layered structures were obtained and analysed.

Finally, sandwich structures formed by two external alumina tapes joined by the multilayer systems built by EPD were fabricated and their mechanical behaviour has been analysed.

2. Experimental

Powders of alumina (α-Al_2O_3, Condea HPA05, USA) and titania (TiO_2-anatase, Merck808, Germany) were used as starting materials. Particle size distributions and specific surface areas of the powders were measured with a laser analyzer (Mastersizer S, Malver, UK) and by one point N_2 adsorption (monosorb, Quantachrome, USA), respectively. Al_2O_3 powders have a mean particle size of 0.4 μm and a specific surface area of 10 m^2/g, while TiO_2 powder have a mean particle size of 0.3 μm and a surface area of 9 m^2/g. The powder density was determined with a He-multipicnometer (Quantachrome, USA), being 3.96 and 3.87 g/cm^3 for Al_2O_3 and TiO_2, respectively.

Zeta potentials of pure Al_2O_3 and TiO_2 suspensions were measured, by microelectrophoresis using a Zeta Meter 3.0 (Zeta-Meter, USA). Suspensions with 0.1 g/l of Al_2O_3 or TiO_2 were prepared using ethanol (Technical grade, 97 vol.% of purity) as solvent and polyethylene imine (PEI, Aldrich, Germany) as dispersing agent. PEI concentrations ranging from 0 to 1 wt.% related to the solids loading were considered. Suspensions were ultrasonically dispersed using a 400 W sonication probe (IKA U400S, Germany) for 2 min and then stirred overnight before zeta potential was measured.

Stabilized ethanol suspensions of compositions 100 vol.% Al_2O_3 (A) and 50 vol.% Al_2O_3/50 vol.% TiO_2 (AT) (50.6 wt.% Al_2O_3 and 49.4 wt.% TiO_2) were prepared to final solids contents of 3 vol.%. Similarly as for zeta potential measurements, suspensions were sonicated and stirred before EPD. Al_2O_3 and TiO_2 suspensions were first dispersed separately before mixing them to prepare AT suspensions. A power source (AMEL mod. 551, Great Britain) capable to work in galvanostatic and potentiostatic mode was used for EPD. Electrophoresis was performed in galvanostatic mode applying constant current densities ranging from 40 to 240 μA/cm^2 for 300 s. Once the optimum current density was determined, the EPD kinetics of A and AT suspensions was studied. The amount of material deposited was quantified in terms of mass per unit of coated area after the drying of the films.

Table 2
Characteristics of the layered structures shaped by EPD on alumina substrates: number of layers, sequences and times of deposition of the A and AT suspensions and total deposition times

Num. layers	EPD sequence	Time/suspension (s)				Time (s)
		AT	A	AT	A	
3	VIII	180	180	180		540
4		180	180	180	180	720
3	IX	60	60	90		210
4		60	60	90	180	390

Graphite foils (99.8 wt.% of purity, Groupe Carbone Lorraine, France) were selected as electrodes in order to optimize the electric conditions of the electrophoretic coating process. The graphite work and counter electrodes (WE and CE) were maintained at a separation distance of 2 cm. The total immersion area of the substrates was twice 2.5 cm × 2.5 cm. The substrates withdrawal was performed with a lift at a constant rate of 7.5 mm/s. Layered structures were obtained by sequential EPD tests alternating the deposition of A and AT slips (deposition sequence: A/AT/A/. . ./AT/A). The amount of mass deposited and, therefore, the thickness of the layers was controlled by the deposition time. For microstructural and mechanical studies, self-supported layered films and sandwich structures were designed and fabricated following the processing routes described in the flow chart of Fig. 1. Tables 1 and 2 summarize the number of layers, and the sequences and times of deposition of the A and AT suspensions used to obtain the designed structures; additionally, monolithic specimens of A and AT compositions were fabricated to study the evolution of the layers independently of the structures.

Self-supported layered films were obtained by EPD using graphite as substrate (Fig. 1a, route (1)), and subsequent drying (24 h at room conditions) and thermal treatment in air at 800 °C–1 h (heating and cooling rates of 5 °C/min) to burn out the graphite. Layered materials with three, five, seven and nine layers, alternating thick A and thin AT layers, were obtained after sintering (Table 1, sequences I–VII).

Table 1
Characteristics of the layered structures shaped by EPD on graphite substrates: number of layers, sequences and times of deposition of the A and AT suspensions and total deposition times

Num. layers	EPD sequence	Time/suspension (s)									Time (s)
		A	AT	A	AT	A	AT	A	AT	A	
3	I	240	20	240							500
5		240	20	240	20	240					460
7		240	20	240	20	240	20	240			1020
9		240	20	240	20	240	20	240	20	240	1280
3	II	180	20	180							380
5		180	20	180	20	180					580
7		180	20	180	20	180	20	180			780
9		180	20	180	20	180	20	180	20	180	980
7	III	180	15	120	15	120	15	180			645
7	IV	180	20	120	20	120	20	180			660
9	V	180	15	120	15	120	15	120	15	180	780
7	VI	240	15	180	15	180	15	240			885
7	VII	420	20	420	20	420	20	420			1740

Fabrication of the ceramic structures for mechanical testing (Fig. 1a, route (2)) was performed by using pre-sintered alumina tapes as substrates glued to the graphite foils in such a way that deposition of particles in the back-faces was avoided as much as possible. Alumina substrates (≈25 mm × 25 mm surface and 400 μm thick) were prepared by cutting cast tapes, obtained as described elsewhere,[12] and pre-sintered at 900 °C–1 h, temperature lower than that for the acceleration of shrinkage (≈1050 °C) for compacts of the alumina used. The open porosity of the alumina substrates was ≈20–25 vol.%.

Four kinds of layered films were deposited on the alumina substrates (Table 2) using two different sequences (VIII and IX) and number of layers (three and four). To fabricate the materials, two alumina substrates with layered films deposited using the same sequence, each one with a different number of layers, were stacked by putting in contact the EPD films (Fig. 1b) and co-sintered using a small load (≈115 g) on top of the combined structure. The thermal treatment promoted the joining of the layered structures sandwiched between the two alumina substrates.

A two-step sintering schedule (1200 °C–4 h and 1450 °C–2 h, heating and cooling rates 2 °C/min) was used in all cases. Polished cross-sections of all materials were covered with Ag and observed by Field Emission Gun Scanning Electron Microscopy with Energy Dispersive X-Ray Spectrometry (FEG-SEM-EDX, Hitachi, S-4700, Japan).

"As sintered" specimens (≈15 mm × 30 mm surface and 800 μm thick) fabricated using alumina as substrate were tested in three point bending using stainless steel supports and an universal testing machine (20 mm span, 0.5 mm min^{-1}; Microtest, Spain) and the fracture surfaces were analysed by FEG-SEM. Three specimens were tested for each studied structure.

3. Results and discussion

3.1. Optimization of EPD conditions

Fig. 2 shows the values of zeta potential of suspensions of the Al_2O_3 and TiO_2 powders used as a function of the concentration of dispersant (PEI). Both powders developed positive surfaces in ethanol (0% PEI), improving the suspension stability when PEI was added. Values for TiO_2 were always lower than for Al_2O_3, indicating that the Al_2O_3 suspensions would have higher electrophoretic mobility than those of TiO_2.

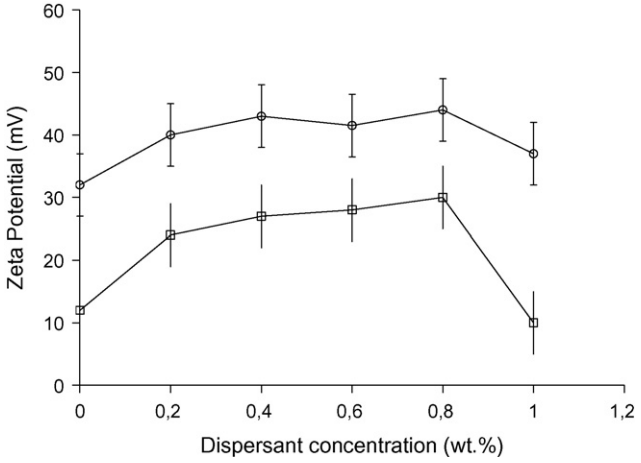

Fig. 2. Zeta potential of Al_2O_3 and TiO_2 suspensions in ethanol.

Maximum values of zeta potential for Al_2O_3 (≈43 mV) were found for additions from 0.4 wt.% of PEI for whereas for TiO_2 they increased for PEI additions up to 0.8 wt.% to a maximum value of 28 mV. Zeta potential decreased sharply for PEI additions higher than 0.8 wt.% for both suspensions, revealing a significant decrease of the slip stability. In order to optimize stability, the minimum PEI additions that maximized zeta potential (0.4 and 0.8 wt.% for Al_2O_3 and TiO_2 suspensions, respectively) were selected for EPD processing.

The deposition on the graphite substrates for the Al_2O_3 (A) and $Al_2O_3 + TiO_2$ (AT) suspensions was evaluated as a function of the applied electric field; the growth of the AT films was faster than that of the A ones. Taking into account that the mobility of the TiO_2 particles was lower than that of the Al_2O_3 ones (Fig. 2) and that the conductivities of both suspensions were similar (≈0.5 μS/cm), the TiO_2 particles appear to have the largest sticking ability.[13] The films obtained applying electric fields higher than 4 V/cm showed surface heterogeneities; hence, an electric filed of 3.6 V/cm between electrodes was chosen as a compromise between high growth rate and film quality for further work.

Fig. 3 plots the growth rate of A and AT films on graphite and alumina substrates for the same applied electric field (3.6 V/cm), when current densities of 8 and 6.4 $\mu A/cm^2$ were respectively applied for deposition times up to 600 s. Kinetics of deposition on the alumina non-conductive substrate was lower than on graphite, suggesting a less effective deposition by electrophoresis on non-conductive substrates. In order to determine deposition yields, the theoretic kinetics for the A suspension were calculated using the theoretical equation for EPD kinetics,[13] the experimental conditions (3 vol.% solids loading, 3.6 ± 0.1 V/cm applied electric field) and the electrophoretic mobility[1] under optimized conditions (0.4 wt.% of PEI) for the Al_2O_3 particles ($6.0 \pm 0.5 \times 10^{-3}$ cm^2/sV).[14] The calculated straight line is also plotted in Fig. 3. From these values and the experimental ones, the sticking parameter on graphite substrates can be estimated, with that of the AT suspension ($f \sim 0.9$) being higher than that of A ($f \sim 0.6$). Similarly, the AT deposition kinetics on the alumina substrates was faster than that of A. For both substrates, the high sticking ability of TiO_2 increased the sticking parameter of the AT suspensions as compared to that of A, leading to a more efficient deposition.

The enlarged plot shown in Fig. 3b demonstrates that mass gain from dipping (zero deposition time) was more efficient for the alumina substrates than for graphite for both suspensions. As a difference to the graphite substrates, the presence of open porosity in the alumina substrates led to two processes

[1] Electrophoretic mobility has been calculated applying the Smoslouski approximation, considering the dielectric constant of ethanol, $\varepsilon_r = 24.3$, and the ethanol viscosity, $\eta = 1003$ mPa s at room conditions.

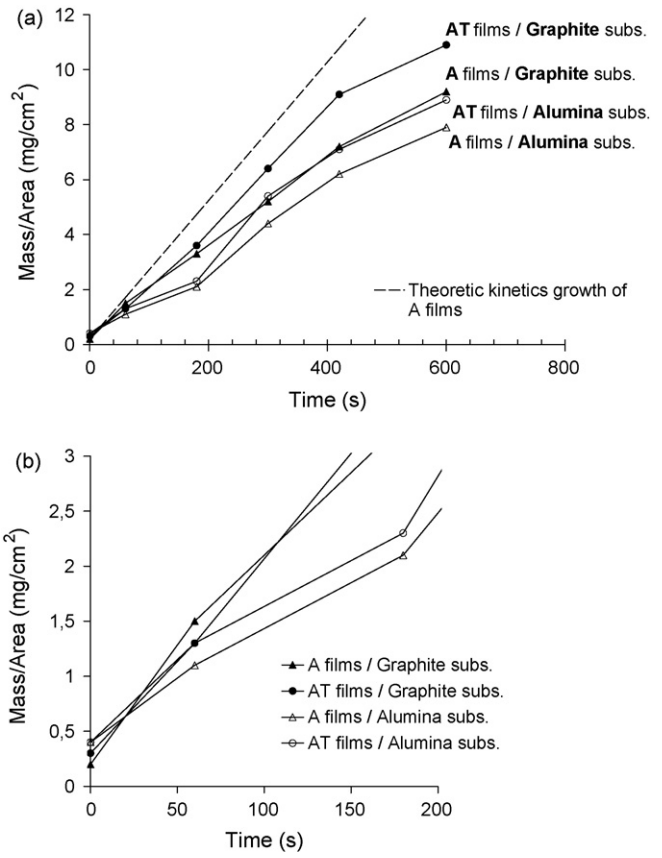

Fig. 3. Kinetics of deposition of the Al_2O_3 (A) and $Al_2O_3 + TiO_2$ (AT) suspensions on the graphite and alumina substrates for an applied electric field of 3.6 V/cm. The mass deposited for unit area of substrate is plotted as a function of deposition time. The dashed lines correspond to the values calculated from the experimental parameters for the A suspension. (a) Complete studied time interval. (b) Detail for short deposition times.

responsible for increased mass gains during dipping into the suspensions: the infiltration of particles and the formation of a wall at the substrate surface by solvent filtration into porous alumina.

Fig. 4 shows the microstructure of the AT sintered self-supported films obtained when a current density of 6.4 μA/cm^2 was applied for 420 s. It was constituted by a continuous matrix of Al_2TiO_5 composition (56.1 wt.% Al_2O_3–43.9 wt.% TiO_2) as revealed by qualitative EDX analysis (56–60 wt.% of Al_2O_3 46–40 wt.% of TiO_2) in which pure TiO_2 particles were homogeneously distributed. Accordingly, the average EDX analyses of the films revealed significant TiO_2 excess (22–26 wt.% of Al_2O_3 and 78–74 wt.% of TiO_2) when compared to the starting composition of the AT suspension (50.6 wt.% Al_2O_3–49.4 wt.% TiO_2), thus verifying the more effective deposition of TiO_2 particles by EPD discussed above (Fig. 3).

3.2. Design and processing of the layered structures

The layered materials were processed using the procedures summarised in Fig. 1 (routes (1) and (2)) and the deposition sequences described in Tables 1 and 2. Deposition times selected to shape AT films in graphite or alumina substrates were selected taking into account the faster deposition of TiO_2 suspension and its capability to enter into the porous Al_2O_3 structure discussed below.

In Fig. 5 the final mass values as a function of total deposition times for the different deposition sequences on graphite (Fig. 5a) and alumina (Fig. 5b) substrates are plotted.

3.2.1. Self-supported structures on graphite substrates

The layered structures envisaged in the present work had to be constituted by relatively thick alumina layers and very thin composite AT layers. Therefore, taking into account the extremely high sticking parameter of the AT suspension as compared to that of A (Fig. 3), layered structures with very short deposition times for AT as compared to those for A were fabricated using graphite as substrate (sequences I to VII, Table 1). In spite of the higher sticking parameter of suspension AT, the deposition kinetics for all layered structures was similar to that of the A suspension (Fig. 3a) because it was the major constituent of the structures.

All the self-supported sintered films were constituted by the envisaged number of layers, as shown in the low magnification micrographs of polished surfaces of self-supported sintered films corresponding to sequences V and VII, in Fig. 6. The structures were formed by dense and relatively thick layers, whose central

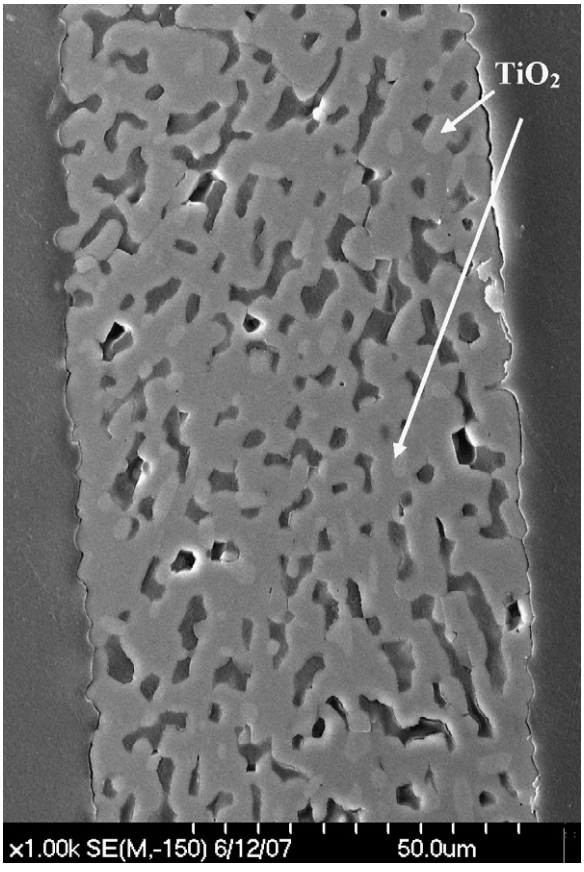

Fig. 4. Microstructure of the AT self-supported sintered specimens. Characteristic view of a polished cross-section. Semi-quantitative EDX analyses gave 56–60 wt.% of Al_2O_3 and 46–40 wt.% of TiO_2 and for the continuous grey phase and more than 98 wt.% of TiO_2 for the white particles (arrows).

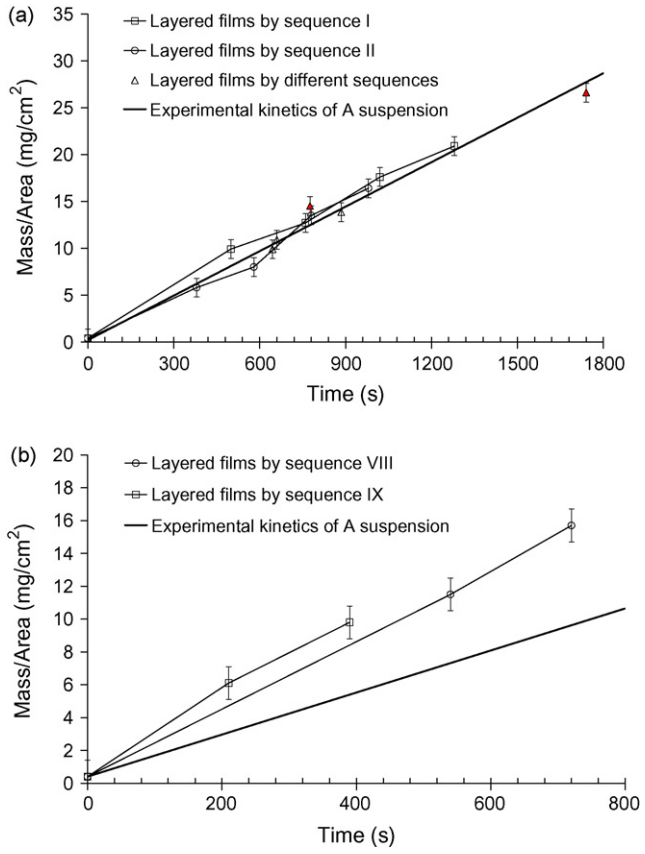

Fig. 5. Deposition kinetics of the layered structures. Deposited mass per unit area is plotted as a function of total deposition times for the different sequences and substrates (Fig. 1 and Tables 1 and 2). The deposition kinetics for A suspensions is plotted as term of comparison. (a) Graphite substrates. The sequences for which values are plotted are indicated. (b) Alumina substrates.

parts were constituted by Al_2O_3 ($TiO_2 < 2$ wt.%), separated by highly porous thin layers with variable relative TiO_2 amounts (40–60 wt.%) that in many cases were higher than those present in the initial AT suspension (43.9 wt.%). These layers could be identified with the original pure Al_2O_3 and composite layers formed by EPD on the graphite substrates.

Longer deposition times of the A suspension led to more uniform thicknesses of the Al_2O_3 layers in the sintered structures whereas, for the range of deposition times used for AT, the Al_2O_3/TiO_2 layers in all structures were reduced to 5–7 μm thickness porous films.

The presence of TiO_2 in relative amounts higher than correspond to the composition of the AT suspension in certain areas of the porous layers shows that preferential deposition of TiO_2 as compared to that of Al_2O_3 took place, as expected from data in Fig. 3.

The decrease of the amounts of TiO_2 from the porous layers towards the Al_2O_3 layers (Fig. 7) was not sharp and, moreover, traces of TiO_2 (<2 wt.%) were found at the centres of the internal Al_2O_3 layers that were sandwiched between two TiO_2-rich ones, revealing that diffusion of TiO_2 during sintering occurred, as reported for other layered alumina–aluminium titanate materials.[6,7] This process would be partially responsible for the porous structure of the TiO_2-rich layers as well as for their extremely small thickness independent from the deposition times.

3.2.2. *Mechanically resistant structures on alumina substrates*

On the basis of the above discussed results two different mechanically resistant structures were designed. Both were EPD layered structures sandwiched between two alumina cast tapes used as substrates (Fig. 1b). After deposition of the layered structures, the substrates were stacked by putting in contact the EPD films. In order to get optimum co-sintering taking profit of TiO_2 diffusion into Al_2O_3 and the reactive sintering of both compounds to form Al_2TiO_5, the first EPD layers on both substrates were always formed from AT suspension whereas the last ones, to be located in contact for sintering, were each one of a different composition, A and AT, respectively.

Taking into account that TiO_2 would migrate into the cast alumina tapes during sintering, much larger deposition times than in the case of graphite and similar to those used for A were used for the deposition of the AT suspension (Table 2). Contrary to what happened when graphite was used as substrate (Fig. 5a), values of deposited mass of the layered films on the alumina substrates were significantly higher than those for the pure A suspension for the two sequences used (Fig. 5b). This fact is due to the increase for layered systems of the extra contributions of wall formation and solvent filtration to EPD on the porous alumina substrates discussed above. The sequential EPD would involve the sample withdrawal and later drying a number of times equal to the number of deposited layers. Hence, the filtration of the suspension and the evaporation of the solvent would lead to wall formation a number of times also equal to the number of layers, increasing the weight gain.

As a difference with the materials obtained from EPD layers deposited on graphite (Figs. 6 and 7) it was not possible to identify the original EPD structure in the polished sections of the sintered materials fabricated from structures VIII and IX. Far from the central parts of the sandwiched structures the pure alumina composition and the dense alumina microstructure of the original tapes was found whereas layers of different composition and porosity levels were observed at the central parts of the specimens. Neither the number nor the thickness of those layers could be straightforward associated with the EPD layers, as discussed below for the sintered materials fabricated using sequence VII that was formed by the thickest layers (Table 1, Fig. 1b).

The characteristic features of the structures formed by the thickest layers are shown in Fig. 8. At the centre of the sandwich structures, three Ti-rich parallel layers with different porosity levels and thicknesses separated by two dense Al-rich layers were found. The thickest (≈16 μm) porous layers were located at the centre and presented the highest TiO_2 amounts (≈40 wt.% of TiO_2); they were surrounded by two dense Al_2O_3 (<Ti-rich 1 wt.% TiO_2) layers of similar thicknesses (≈20 μm). The other two porous layers presented similar amounts of TiO_2 (≈18–25 wt.%) and were located contiguous to the central Al_2O_3 layers.

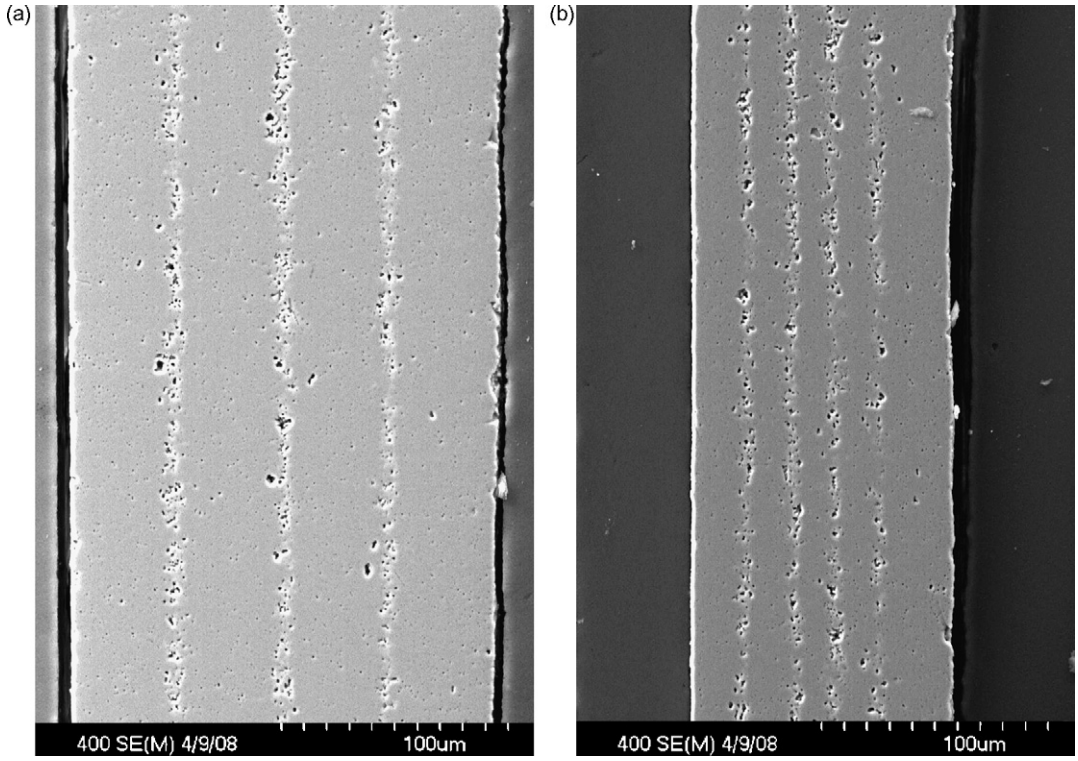

Fig. 6. General views of the self-supported sintered films. The sense of growth during the shaping process was from the left to the right of the micrograph (i.e., the fist A deposited layer corresponds to the layer located at the left). FE-SEM micrographs of polished sections. (a) Sequence VII in Table 1. (b) Sequence V in Table 1.

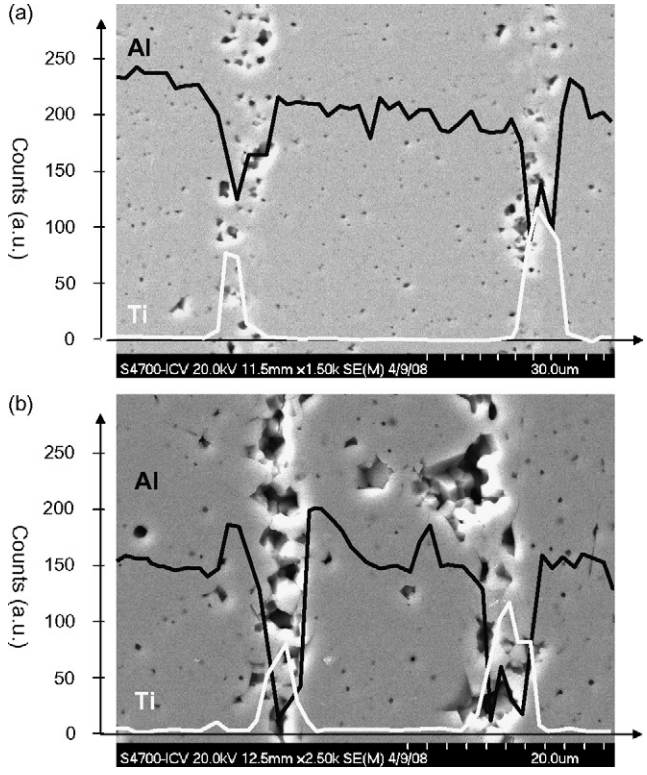

Fig. 7. Details of the central parts of the self-supported sintered films shown in Fig. 6 together with qualitative chemical analyses. FE-SEM-EDX of polished sections. (a) Sequence VII in Table 1. (b) Sequence V in Table 1.

Taking into account the original green structure (Fig. 1b), the thinnest composite layers and the dense Al_2O_3 ones observed in the sintered materials would correspond to the evolution during sintering of the first AT and A layers deposited on the tapes (AT1 and AT1′; A1 and A1′, Fig. 1b), respectively. Thus, the central composite ones would be the result of the combination of layers AT2, A2 and AT2′, in fact, this layers presented the highest TiO_2 amounts. As discussed above for the self-supported layered specimens, the decrease of Ti from the centre of the thin composite layers towards the Al_2O_3 ones was not sharp (Fig. 8) due to TiO_2 diffusion towards the original tape as well as towards the EPD Al_2O_3 layers.

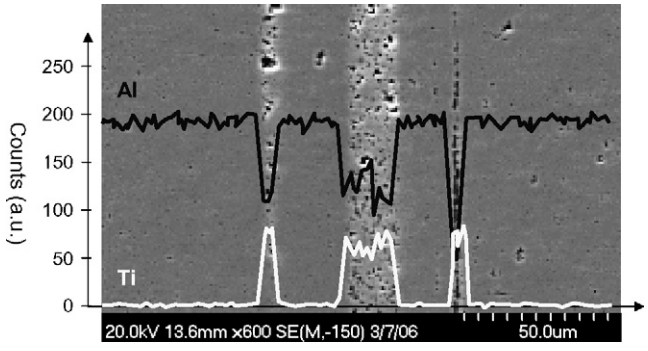

Fig. 8. Characteristic features of the sintered specimens fabricated using alumina tapes as electrodes. Micrograph of the central part of a specimen processed using sequence VIII (thick layers) together with qualitative chemical analyses. FE-SEM-EDX of a polished section.

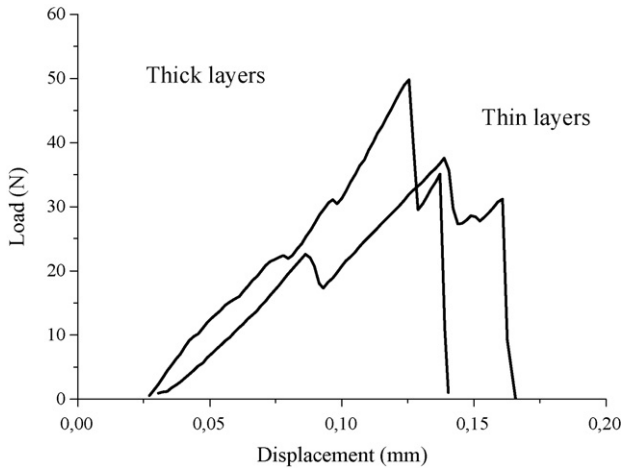

Fig. 9. Characteristic load-displacement of the load frame curves for specimens tested in three points bending. Labels correspond to the two kinds of structures studied. Thin layers: sequence IX, Table 1. Thick layers: sequence VIII, Table 1.

The characteristic features of the microstructures of specimens with thinner layers (sequence IX, Table 1) were similar to these just described for the films with thick layers the only difference being the relative TiO_2 contents of the layers. The amounts of TiO_2 in the porous layers located close to the alumina tapes that corresponded to the AT1 and AT1′ layers were ≈25–30 wt.%, up to 5 wt.% of TiO_2 was found in the alumina layers A1 and A1′ and the central porous layers contained 40–50 wt.% of TiO_2. The differences in TiO_2 amounts are due to the easier distribution of TiO_2 when thinner layers are involved.

Fig. 9 shows characteristic load-displacement curves for the two studied structures. Even though these are only preliminary results and more testing should be performed in systems different from sandwich, some general remarks can be done. Both materials presented graceful fracture with differentiated load drops prior to the complete failure. When comparing the structures between them, the presence of thinner layers led to structures with higher capacity for strain, as shown by the larger displacements at the point of fracture

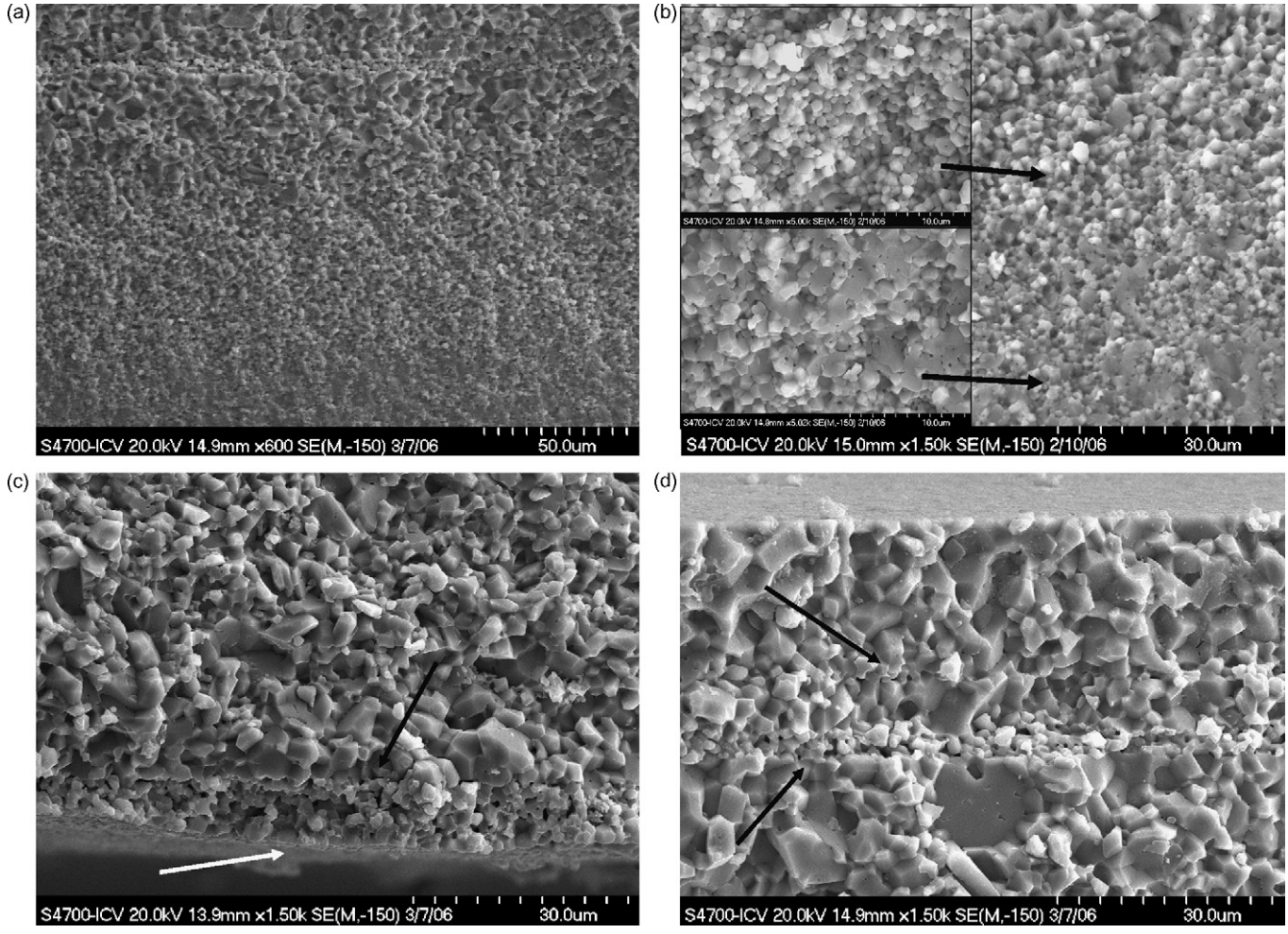

Fig. 10. Characteristic features of the fracture surfaces of the studied laminates. Specimen constituted by thick internal layers (sequence VIII, Table 2). FE-SEM. (a) General view. The bottom part of the micrographs corresponds to the green tape with four EPD layers. (b) Detail of the transition between the original tape presenting mixed trans/inter fracture (bottom) and the zone of predominantly intergranular fracture. Higher magnification micrographs of both zones are shown at the left part of the figure. (c and d) Details of the central zone close to the tapes originally with four (c) and three (d) EPD layers. The arrows point to the linear porous zones rich in Ti, AT1, AT2 and AT1′. Different fracture planes and delamination are observed across the zones rich in Ti.

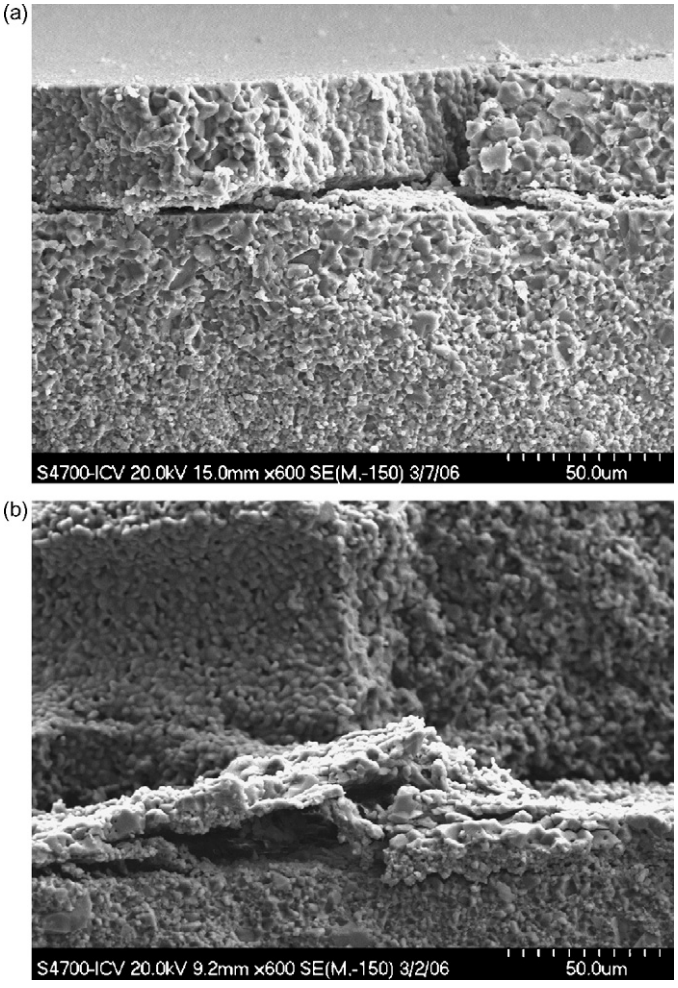

Fig. 11. Effect of the thickness of the original alumina EPD layers in the fracture. FE-SEM micrographs of fracture surfaces. (a) Specimen constituted by thick internal layers (sequence VIII, Table 2). (b) Specimen constituted by thin internal layers (sequence IX, Table 2).

attained whereas thicker layers led to higher ultimate failure loads.

Different failure modes associated to different microstructural developments were observed in the fracture surfaces, as shown in Figs. 10 and 11. The microstructural developments were consequence of the original green structures combined with the changes associated to the diffusion of TiO_2 into the pure alumina tapes and EPD layers, and led to different failure modes as observed in alumina/aluminium titanate laminates obtained by slip casting[6,7] in which TiO_2 diffusion led to alumina grain growth and a change from mixed trans/intergranular fracture to purely intergranular.

In Figs. 10 and 11, the characteristic features of the fracture surfaces of specimens constituted by thick layers (sequence VIII, Table 1) are shown. In which follows, the description of the fracture features starts from the tape that originally had four EPD layers (Fig. 1b).

Far from the central part of the samples, the original alumina tapes (Figs. 8 and 10) of grain size between 1 and 2 μm (Fig. 10b) presented mainly transgranular fracture (Fig. 10a and b). Then fracture became progressively intergranular and the grain size increased towards the central parts of the specimens (Fig. 10a, c, and d), reaching extremely large sizes (up to $15 \approx \mu m$). Then, the grain size suddenly become very small (<1 μm, Fig. 11c and d) along layers that could be identified with the Ti-rich thin ones observed in the polished specimens, AT_1 and AT_1' (Fig. 8). Partial delamination occurred across those porous composite layers (Fig. 10d) that were the weakest. The central parts of the specimens, formed by the two dense alumina layers plus the porous central composite one, presented different fracture planes as if they had acted as load bearing constituents after delamination and before the complete failure (Figs. 10c and 11a). In the central parts of the laminated specimens formed by thick layers there were not found distinct delamination planes following the interfaces of the constituent layers or the central composite layers (Fig. 11a). On the contrary, delamination through the thin and porous layers located at the central parts of the specimens was observed in the laminates formed by thin layers, the intermediate layers acting as ligaments, as shown in Fig. 11.

Large portions of the central parts of the laminates with thicker layers remained un-fractured while multiple delaminations were observed in the central parts of the specimens with thinner layers that presented wood-like fracture (Fig. 11b). These fracture modes were reflected in the load-displacement curves as higher loads were needed to fracture the more resistant thicker ligaments whereas larger displacements were admitted by the specimens with thinner layers due to multiple delaminations.

These results demonstrate the viability of very thin-layered structures based on alumina–titania with high capacity for strain before failure. Optimization of these structures would have to consider the fact that a compromise has to be reached in order to maximize strain while keeping sufficient strength.

4. Conclusions

The processing parameters to fabricate alumina–aluminium titanate structures formed by thick self-supported alumina tapes (400 μm) joined together by layered alumina–aluminium titanate structures shaped by electrophoretic deposition (EPD) have been established.

The optimisation of the stability of alumina and alumina–titania suspensions in ethanol and the EPD parameters allows the shaping of homogeneous and well defined layered structures on two different substrates, graphite and alumina. The study of the evolution of self-supported structures obtained on graphite substrates leads to the design of more complex materials as the two sandwich structures formed by external alumina tapes joined by multilayer systems built by EPD characterized in this work.

The designed materials present graceful fracture associated to the layered internal structure. Thicker layers lead to higher loads needed to fracture the more resistant thicker ligaments and larger displacements are admitted by the specimens with thinner layers due to multiple delaminations.

Acknowledgment

The authors would like to acknowledge the support of the Project MEC MAT2006-13480 C02, Spain.

References

1. Clegg, W. J., Kendall, K., Alford, N. McN., Birchall, J. D. and Button, T. W., A simple way to make tough ceramics. *Nature*, 1990, **347**, 45–57.
2. Clegg, W. J., Design of ceramics laminates for structural applications. *Mater. Sci. Technol.*, 1998, **14**(6), 483–495.
3. Zhang, J. X., Jiang, D. L., Qin, Sh. Y. and Huang, Zh. R., Fracture behavior of laminated SiC composites. *Ceram. Int.*, 2004, **30**, 697–703.
4. Tomaszewski, H., Weglarz, H., Wajler, A., Boniecki, M. and Kalinski, D., Multilayer ceramic composites with high failure resistance. *J. Eur. Ceram. Soc.*, 2007, **27**(2–3), 1373–1377.
5. Chan, H. M., Layered ceramics: processing and mechanical behavior. *Annu. Rev. Mater. Sci.*, 1997, **27**, 249–282.
6. Bueno, S. and Baudín, C., In situ developed layers with dissimilar microstructures in alumina–aluminium titanate laminates. *J. Mater. Sci.*, 2006, **21**, 3695–3700.
7. Bueno, S. and Baudín, C., Layered materials with high strength and flaw tolerance based on alumina and aluminium titanate. *J. Eur. Ceram. Soc.*, 2007, **27**(2–3), 1455–1462.
8. Bueno, S. and Baudín, Design and processing of a ceramic laminate with high toughness and strong interfaces, *Composites B*, submitted for publication.
9. Bueno, S. and Baudín, Oxide ceramic laminates presenting graceful fracture, submitted for publication.
10. Besra, L. and Liu, M. L., A review on fundamentals and applications of electrophoretic deposition (EPD). *Prog. Mater. Sci.*, 2007, **52**(1), 1–61.
11. Besra, L., Compson, C. and Liu, M. L., Electrophoretic deposition of YSZ particles on non-conducting porous NiO-YSZ substrates for solid oxide fuel cell applications. *J. Am. Ceram. Soc.*, 2006, **89**(10), 3003–3009.
12. Gurauskis, J., Sánchez-Herencia, A. J. and Baudín, C., Joining green ceramic tapes made from water-based slurries by applying low pressures at ambient temperature. *J. Eur. Ceram. Soc.*, 2005, **25**(15), 3403–3411.
13. Sarkar, P. and Nicholson, P. S., Electrophoretic deposition (EPD): mechanisms, kinetics, and application to ceramics. *J. Am. Ceram. Soc.*, 1996, **79**(8), 1987–2002.
14. Moreno, R., The role of slip additives in tape casting technology. I. Solvents and dispersants. *Am. Ceram. Bull. Soc.*, 1992, **71**(10), 1521–1531.